

6-2004

Air-coupled, focused ultrasonic dispersion spectrum reconstruction in plates

Stephen D. Holland
Iowa State University, sdh4@iastate.edu

Sorin V. Teles
Iowa State University

Dale E. Chimenti
Iowa State University

Follow this and additional works at: http://lib.dr.iastate.edu/aere_pubs

 Part of the [Aerospace Engineering Commons](#)

The complete bibliographic information for this item can be found at http://lib.dr.iastate.edu/aere_pubs/5. For information on how to cite this item, please visit <http://lib.dr.iastate.edu/howtocite.html>.

This Article is brought to you for free and open access by the Aerospace Engineering at Iowa State University Digital Repository. It has been accepted for inclusion in Aerospace Engineering Publications by an authorized administrator of Iowa State University Digital Repository. For more information, please contact digirep@iastate.edu.

Air-coupled, focused ultrasonic dispersion spectrum reconstruction in plates

Abstract

This paper presents and demonstrates a noncontact method for measuring the Lamb wave dispersion spectrum of a plate. Noncontact air-coupled source and receive transducers are used with line-focus mirrors and 50–700 kHz broadband apparatus for simultaneous measurement over a broad spectrum of refractive angles and multiple guided modes. Broadband, wide-angle wave forms are measured as a function of position. The Fourier transform of these wave forms from the $t - x$ domain to the $v - k$ domain gives an approximate spectrum of the dispersion relation. We measure the dispersion spectra of Lucite™, aluminum, balsa wood, and a carbon fiber epoxy laminate, and show that the measured spectra agree well with the dispersion relation calculated from Lamb wave theory.

Keywords

nondestructive evaluation, nondestructive testing, Lamb waves, Lamb wave theory

Disciplines

Aerospace Engineering

Comments

This article was originally published in the *Journal of the Acoustical Society of America* 115, no. 6 (June 2004): 2866–2872, doi:[10.1121/1.1710501](https://doi.org/10.1121/1.1710501).

Air-coupled, focused ultrasonic dispersion spectrum reconstruction in plates

Stephen D. Holland^{a)} and Sorin V. Teles

Center for Nondestructive Evaluation, Iowa State University, Ames, Iowa 50011

D. E. Chimenti

Department of Aerospace Engineering and Center for Nondestructive Evaluation, Iowa State University, Ames, Iowa 50011

(Received 1 July 2003; accepted for publication 1 March 2004)

This paper presents and demonstrates a noncontact method for measuring the Lamb wave dispersion spectrum of a plate. Noncontact air-coupled source and receive transducers are used with line-focus mirrors and 50–700 kHz broadband apparatus for simultaneous measurement over a broad spectrum of refractive angles and multiple guided modes. Broadband, wide-angle wave forms are measured as a function of position. The Fourier transform of these wave forms from the $t-x$ domain to the $\omega-k$ domain gives an approximate spectrum of the dispersion relation. We measure the dispersion spectra of Lucite™, aluminum, balsa wood, and a carbon fiber epoxy laminate, and show that the measured spectra agree well with the dispersion relation calculated from Lamb wave theory. © 2004 Acoustical Society of America. [DOI: 10.1121/1.1710501]

PACS numbers: 43.35.Cg, 43.35.Ns, 43.20.Gp, 43.35.Zc [RLW]

Pages: 2866–2872

I. INTRODUCTION

Air-coupled ultrasonic materials characterization has been in use since the 1970s, but has not been widely used until recently because of the unavailability of commercial systems. Modern air-coupled ultrasonics began with the development of the capacitive ultrasonic transducer by Kuhl *et al.*¹ in 1954. Luukkala *et al.*² in 1971 used capacitive transducers to infer the dispersion of guided modes in plates by identifying peaks in transmission as a function of incident angle. While this led to an approximate estimation of dispersion, it was limited in its precision by interference from sidelobes of the transducer. Safaeinili *et al.*³ in 1995 introduced both synthetic aperture scanning, which factors out sidelobe interference, and model-based prediction to yield a precision measurement of the dispersion relation of a sample. By 1995, air-coupled ultrasound was established as a qualitative tool for defect imaging, with development culminating in the release of a commercial air-coupled ultrasonic system,⁴ which made narrowband air-coupled ultrasonic measurement broadly accessible as a research tool. Schindel *et al.*⁵ developed in 1995 broadband micromachined capacitive air-coupled transducers, making truly broadband air-coupled measurements possible. In 1996 Ladabaum and Khuri-Yakub⁶ introduced high frequency micromachined air-coupled transducers with sensitivity as high as 11.4 MHz. In 2002 Hosten and Castaings⁷ used a parabolic mirror and chirp excitation for measuring the phase velocity of Lamb modes.

We apply the water-coupled two-dimensional Fourier transform method of Fei and Chimenti⁸ and the parabolic mirror of Hosten and Castaings⁷ to air-coupled measurements of dispersion spectra. We provide theoretical justifica-

tion for our method and show that, unlike previously used air-coupled dispersion methods, it decouples transducer artifacts from the measured data.

We present a method for the reconstruction of the transmission coefficient of a plate and its related guided wave mode dispersion spectrum using highly focused, broadband air-coupled ultrasound both for generation and detection. We apply pulse compression techniques to maximize signal-to-noise ratio, but insonify with a novel burst of temporally and spectrally tailored random phase noise rather than the more conventional chirp excitation. Stepwise scanning of the transmitted field, followed by a spatial-temporal two-dimensional Fourier transform, yields a reconstruction of the plate transmission coefficient. In the following we summarize our theory and procedure and present measured transmission coefficient results, displayed as grayscale image data, from samples of aluminum, Lucite™, carbon fiber epoxy laminate, and wood plates. Corresponding guided wave mode curves calculated from known geometric, density, and elastic parameters are compared to the experimental data and found to be in close agreement.

II. THEORY

Previous papers analyzing air-coupled plate mode propagation, such as Safaeinili *et al.*,³ model the plate as a transmission coefficient that operates on the plane wave spectrum of piston transducers. Safaeinili *et al.* showed that a pair of piston transducers can be very closely modeled with a pair of Gaussian transducers, and therefore it is common to model piston transducers as Gaussian. A Gaussian transducer model allows the use of the complex transducer point⁹ to mathematically replace a distributed Gaussian transducer with a point transducer spatially displaced into the complex plane.

^{a)} Author to whom all correspondence should be addressed; electronic mail: sdh4@cornell.edu

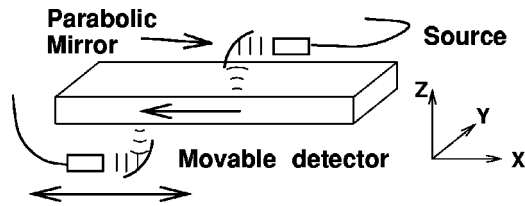


FIG. 1. Diagram of plate with air-coupled transducers and focusing mirrors.

Transducer modeling has been very important because wave form predictions have been used in prior work to calibrate and verify the measurements. In contrast, the results of our dispersion spectra measurements can be directly compared with calculations of Lamb wave modes, because air is a very tenuous coupling medium and only minutely perturbs the Lamb mode dispersion. Since there is no need to include transducer characteristics in those calculations, an empirical transducer model is sufficient for our purposes. We treat our transducer systems (the transducers themselves coupled to focusing mirrors) as sound producing units. Each transducer system is modeled as an arbitrary continuum of point transducers, or equivalently as a generator or detector of an arbitrary spectrum of plane waves. The transducer characteristic, which will be denoted $H(k_x, k_y, k_z, \omega)$, is left as an unknown in the model, and can be measured experimentally.

Our measurement apparatus consists of planar air-coupled thin-film transducers⁵ focused by a cylindrical parabolic mirror to create a focused sheet beam incident on the plate, as illustrated in Fig. 1. The beam can be considered as a spectrum of plane waves containing a broad range of spatial frequencies. At the surface, the plane waves couple into guided modes within the plate. Each mode propagates along the plate and leaks energy into the air. The reradiated field below the plate is measured by a nominally identical detector through another line focus mirror. The detector is scanned stepwise in x parallel to the surface, and the transmitted signal is measured as a function of position and time.

Consider an acoustic point source located at coordinates (x', y', z') in the air. An impulse generated by this point source will, satisfying the wave equation, create a transient spherical pressure wave propagating outward in the surrounding air,

$$f(x, y, z, t) = \frac{1}{r} \delta(r - c_a t) \otimes_t h_s(t), \quad (1)$$

where $r = \sqrt{(x - x')^2 + (y - y')^2 + (z - z')^2}$, c_a is the air wave speed, $h_s(t)$ is the impulse response of the source transducer and electronics, and \otimes_t denotes temporal convolution.

We represent our source transducer system, the transducer and mirror, by a spatial continuum of point sources. The shape of the continuum will be the shape of the source transducer itself distorted into a curve by reflection in the mirror. We give each point in the continuum source a separate impulse response, $h_s(x, y, z, t)$. The pressure wave in the air is then the integral of the effects of each infinitesimal point source, that is the convolution over space and time of the effect of a single source with the source distribution,

$$f(x, y, z, t) = \delta(\sqrt{(x - x')^2 + (y - y')^2 + (z - z')^2} - c_a t) \otimes_{x, y, z, t} h_s(x, y, z, t). \quad (2)$$

This expression for $f(x, y, z, t)$ in Eq. (2) is the pressure wave in the air resulting from the arbitrary source characteristic $h_s(x, y, z, t)$. For our line-focus system of transducer and mirror, we assume that the source transducer has a uniform response over a length l in y , normal to the incident plane as shown in Fig. 1. That is, $h_s(x, y, z, t) = h_s(x, z, t)(u(y + l/2) - u(y - l/2))/\sqrt{2\pi l}$, where $u(y)$ is the spatial unit step in the y direction.

Spectral decomposition [four-dimensional (4D) Fourier transform] of $f(x, y, z, t)$ yields

$$F(k_x, k_y, k_z, \omega) = \frac{4\pi^2}{ik_r c_a} [\delta(\omega/c_a - k_r) - \delta(\omega/c_a + k_r)] \times H_s(k_x, k_z, \omega) \sqrt{\frac{l}{2\pi}} \text{sinc}\left(\frac{k_y l}{2}\right) \times e^{-ik_x x' - ik_y y' - ik_z z'}, \quad (3)$$

where k_x , k_y , and k_z are the x , y , and z spatial wave numbers respectively, $H_s(k_x, k_z, \omega)$ is the Fourier transform of $h_s(x, z, t)$, ω/c_a is the spatial wave number of a plane wave of frequency ω in air, and $k_r \equiv \sqrt{k_x^2 + k_y^2 + k_z^2}$. Equation (3) can be understood very easily by looking at its parts. The 4D Fourier transform of a spherical wave propagating outward from the origin is $4\pi^2/ik_r c_a [\delta(\omega/c_a - k_r) - \delta(\omega/c_a + k_r)]$. The transform of $h_s(x, z, t)$ is $H_s(k_x, k_z, \omega)$. The width and shape of the source transducer in the y (focal line) direction transforms to $\sqrt{l/2\pi} \text{sinc}(k_y l/2)$, and the spatial shift of the source transducer location from the origin to coordinates (x', y', z') is represented by $\exp(-ik_x x' - ik_y y' - ik_z z')$.

Equation (3) allows us to analyze our source as an infinite sum of plane waves, i.e., as a spectral decomposition. It is the spectrum of the acoustic field anywhere in space above the plate. The acoustical effect of the plate is to introduce into this expression a transmission coefficient.¹⁰ The transmission coefficient is the complex ratio of the transmitted pressure divided by the incident pressure of a plane wave. The effect of the transmission coefficient is an amplitude reduction and phase change in the transmitted wave. In particular, it encompasses the effect of resonant guided modes within the plate.³ The pressure wave spectrum below the plate is therefore

$$\frac{4\pi^2}{ik_r c_a} \left[\delta\left(\frac{\omega}{c_a} - k_r\right) - \delta\left(\frac{\omega}{c_a} + k_r\right) \right] \times T(k_x, k_y, k_z, \omega) H_s(k_x, k_z, \omega) \times \sqrt{\frac{l}{2\pi}} \text{sinc}\left(\frac{k_y l}{2}\right) e^{-ik_x x' - ik_y y' - ik_z z'}, \quad (4)$$

where $T(k_x, k_y, k_z, \omega)$ is the transmission coefficient.

As with the source transducer shape and impulse response, the line focus detector transducer can, by reciprocity, be modeled by convolution of the field with the transducer's temporal-spatial response, $h_d(x, y, z, t)$, which yields the measured voltage wave form. Equivalently, spectral domain

multiplication with the Fourier transform of the response, $H_d(k_x, k_y, k_z, \omega)$, provides the spectrum of the measured voltage wave form. As in the case of the source system, we model the detector transducer and line-focus mirror as a single unit with uniform response over its spatial extent l in y , $h_d(x, y, z, t) = h_d(x, z, t)(u(y + l/2) - u(y - l/2))/\sqrt{2\pi l}$, or equivalently in the spectral domain, $H_d(k_x, k_y, k_z, \omega) = H_d(k_x, k_z, \omega)\sqrt{l/2\pi} \text{sinc}(k_y l/2)$.

The spectrum measured by the detector transducer is therefore the pressure wave spectrum of Eq. (4) multiplied by the detector response,

$$V(k_x, k_y, k_z, \omega) = \frac{4\pi^2}{ik_r c_a} \left[\delta\left(\frac{\omega}{c_a} - k_r\right) - \delta\left(\frac{\omega}{c_a} + k_r\right) \right] \times T(k_x, k_y, k_z, \omega) H_s(k_x, k_z, \omega) H_d(k_x, k_z, \omega) \frac{l}{2\pi} \times \text{sinc}^2\left(\frac{k_y l}{2}\right) e^{-ik_x x' - ik_y y' - ik_z z'}. \quad (5)$$

From hereon, for the sake of simplicity we will assume infinite transducer extent in y . As the length l of the transducers along the focal axis goes to infinity (perfect line focus), the k_y dependence can be simplified to a delta function, leaving

$$V(k_x, k_y, k_z, \omega) = \frac{4\pi^2}{ik_r c_a} \left[\delta\left(\frac{\omega}{c_a} - k_r\right) - \delta\left(\frac{\omega}{c_a} + k_r\right) \right] \times T(k_x, k_y, k_z, \omega) H_s(k_x, k_z, \omega) H_d(k_x, k_z, \omega) \times \delta(k_y) e^{-ik_x x' - ik_y y' - ik_z z'}. \quad (6)$$

The voltage measured by the detector transducer at location (x, y, z) is the four-dimensional inverse Fourier transform of Eq. (6),

$$v(x, y, z, t) = \frac{1}{4\pi^2} \int_{\omega} \int_{k_x} \int_{k_y} \int_{k_z} \frac{1}{ik_r c_a} \left[\delta\left(\frac{\omega}{c_a} - k_r\right) - \delta\left(\frac{\omega}{c_a} + k_r\right) \right] \times T(k_x, k_y, k_z, \omega) H(k_x, k_z, \omega) \delta(k_y) \times e^{ik_x(x-x') + ik_y(y-y') + ik_z(z-z') + i\omega t} dk_z dk_y dk_x d\omega. \quad (7)$$

Here we have combined $H_s(k_x, k_z, \omega)H_d(k_x, k_z, \omega)$ into a single composite function $H(k_x, k_z, \omega)$ that represents the combined response of the source and detector transducer systems. Equation (7) gives the time domain signal recorded by our detector in response to an impulse excitation. Because of the presence of delta functions, it is straightforward to perform two of the integrals in Eq. (7). We choose to perform the k_y and k_z integrals, yielding

$$V(x, y, z, t) = \frac{1}{4\pi^2} \int_{\omega} \int_{k_x} \frac{1}{ik_{z0} c_a} T(k_x, 0, k_{z0}, \omega) H(k_x, k_{z0}, \omega) \times e^{ik_x(x-x') + ik_{z0}(z-z') + i\omega t} dk_x d\omega \quad (8)$$

where $k_{z0} \equiv \sqrt{\omega^2/c_a^2 - k_x^2}$, the z component of the air wave vector.

In the processing of our measured data, we will perform a two-dimensional forward discrete Fourier transform in x and t . In the model, we approximate that discrete transform with a two-dimensional forward continuous Fourier transform, leading to

$$V(k_x, y, z, \omega) = \frac{1}{ik_{z0} c_a} T(k_x, 0, k_{z0}, \omega) H(k_x, k_{z0}, \omega) \times e^{-ik_x x' + ik_{z0}(z-z')}. \quad (9)$$

The final step in our processing will be taking the complex magnitude of V ,

$$|V(k_x, y, z, \omega)| = \frac{1}{c_a k_{z0}} |T(k_x, 0, k_{z0}, \omega)| |H(k_x, k_{z0}, \omega)|, \quad (10)$$

which is conveniently independent of both vertical transducer positions, z' and z . It is also independent of the transducer positions along the focal line, y' and y because we have assumed the transducers to be infinitely long. Finally, k_{z0} , as defined earlier, is dependent only on ω , k_x , and c_a , so its dependence can be subsumed into the other parameters. We can write

$$|V(k_x, \omega)| = \frac{1}{c_a k_{z0}} |T(k_x, \omega)| |H(k_x, \omega)|, \quad (11)$$

where $T(k_x, \omega) \equiv T(k_x, 0, k_{z0}, \omega)$ and $H(k_x, \omega) \equiv H(k_x, k_{z0}, \omega)$. Therefore, the measured $V(x, t)$, discrete Fourier transformed to $V(k, \omega)$, is the magnitude of the spectral transmission coefficient T , windowed by the response of the transducers $H(k_x, \omega) = H_s H_d$ and scaled by the reciprocal of the z component of the air wave vector. The simplicity of Eq. (11) allows for very simple analysis. Since maxima in the transmission coefficient correspond to portions of the spectral domain where the plate is in transverse resonance,¹¹ i.e., guided wave modes in the plate, and these maxima thereby indicate the plate dispersion relation,³ we will interpret ridges in $|V(k_x, \omega)|$ as the dispersion curves of guided wave modes. Moreover, Eq. (11) shows that the combined effect of the transducers and mirrors is purely that of a multiplicative window in the (k, ω) domain. In contrast with previous models, this analysis identifies the two-dimensional Fourier transform of the measured voltage to be the transmission coefficient without assuming a particular beam profile, such as Gaussian. Instead it allows either an empirically measured model of the transducer or a calculated model based on the spatial Fourier transform of the shape of the active area. In addition, this analysis can be readily extended to three dimensions, yielding a modified Eq. (11) with k_y dependence added to V , T , and H .

The above-presented analysis is limited by a few assumptions. We implicitly assume an infinite plate, but the real plates we measure are finite. We assume infinitely long line focus transducers, but the transducer assemblies are actually rather narrow. We ignore reflections and reverberations between the transducers and the plate, because these can be eliminated through time windowing. Despite these limita-

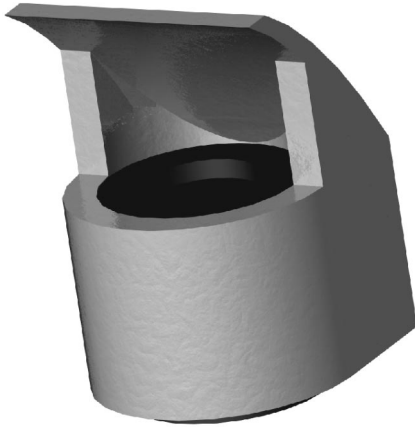


FIG. 2. Line-focus mirror (gray) and transducer (black).

tions, in practice we have found the above-given analysis to be quite satisfactory for interpreting measured data and matching theoretically calculated dispersion curves to experiment.

III. EXPERIMENTAL METHOD

We measure the transmission coefficient of a medium in the geometry shown schematically in Fig. 1 using an effective impulse source (explained later) and a 10 MSPS 12 bit wave form recorder. Time wave forms are recorded as the position x is stepped over a range wide enough for the signal to disappear in noise, giving $V(x, t)$. The measured, windowed transmission function, $|V(k_x, \omega)|$ is calculated from the two-dimensional discrete Fourier transform of $V(x, t)$. The reciprocal of the step size in x determines the largest k_x that can be measured without aliasing. The range traveled in x determines the resolution in k_x , and zero-padding the $V(x, t)$ data reduces pixelation in the $V(k_x, \omega)$ spectrum through interpolation.

The actual transducers that we use are planar (piston radiators). To create line-focus source and detector systems, the planar transducers are coupled to line-focus mirrors. The mirrors, shown in Fig. 2, have been designed with a CAD tool to have the required parabolic shape and are manufactured from Duraform GF (glass-filled polyamide) using a rapid prototyping method to a surface finish better than 5 μm . These mirrors have a sufficient beam angle to excite a 14.4° slice of the useful region of (k_x, ω) space. Because of the low velocity ratio between air and almost any solid, both shear and longitudinal critical angles occur at relatively low values, so a 14.4° beam acceptance angle is sufficient for most measurements. Figure 3 shows the result of the measurement procedure below with vertically aligned transducers and no plate in place. This is the empirical transducer and mirror response window $H(k_x, \omega)$ of Eq. (11). No contrast stretching or histogram equalization has been performed on this or any other image reported in this paper. As seen in Fig. 3, the transducers have a spectral sensitivity width of 14.4° and wideband frequency response. We have measured the system response, including the effects of both transducers, to be centered at 380 kHz with -10 dB points at 169 and 657 kHz. The dispersion measurements themselves tend to be

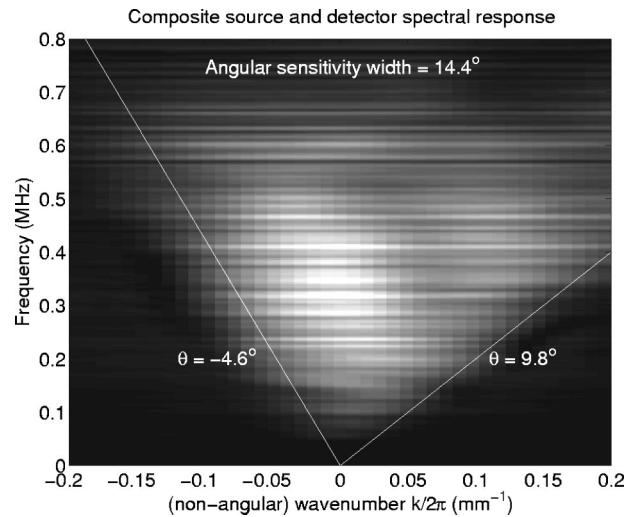


FIG. 3. Spectral sensitivity window of air-coupled transducers and mirrors, $H(k_x, 0, \sqrt{\omega^2/c_a^2 - k_x^2}, \omega)$. Lines are drawn to reflect the beam width.

limited to a somewhat reduced bandwidth because the sensitivity of the measurement drops off with $1/k_{z0}$ [Eq. (11)] which is equivalent to it dropping off with $1/\omega$. The asymmetry visible in Fig. 3 comes from the reflection of the diffraction from the edge of the transducer in the inherently asymmetric parabolic mirror.

Unlike previous methods, we have not had to assume in our analysis a particular physical shape and directivity function of the transducer, except that it is line focus. Instead, we subsumed the transducer shape and directivity into the spectral characteristic of the transducers, $H(k_x, \omega)$, that we empirically measured in Fig. 3. As shown in Eq. (11), $H(k_x, \omega)$ windows the transmission coefficient $T(k_x, \omega)$ in the measurement. The transducer shape and directivity thereby determine which region in (k_x, ω) space is probed by the measurement. In general for a focused transducer, $H(k_x, \omega)$ has the approximate shape of a slice in (k_x, ω) with an angular width that corresponds to the beam acceptance angle of the mirrors and transducers. While we will not attempt to divide out H from our results, this empirical measurement informs us of the effect of the transducer shape on our results, and all measurements are subject to this sensitivity window.

In most of our experiments, we rotate the mirrors about their focal line. Rotating the mirror rotates and stretches the measurement sensitivity window in (k_x, ω) space and allows more modes to be simultaneously excited and measured than possible with unrotated transducers. If the rotated slice is still not large enough to measure all the modes of interest, measurements can be repeated at multiple mirror angles to provide a complete picture of the modal structure built from the sum of rotated copies of the measurement window of Fig. 3.

To maximize the signal-to-noise ratio (SNR), we use a pulse compression technique that simulates an impulse source, equivalent to the autocorrelation of the long, broadband excitation signal. Others have demonstrated similar SNR improvements,¹² but we have developed a random phase excitation wave form to use in place of the usual chirp (linear frequency sweep). The random phase wave form is constructed to have both a desired frequency spectrum and

desired temporal envelope. The wave form is constructed in the frequency domain with the desired amplitude spectrum, but with phases selected using a pseudorandom number generator. The temporal envelope is then applied in the time domain. The desired amplitude spectrum and temporal envelope are inherently contradictory requirements. We apply the two criteria iteratively until a wave form is obtained that very nearly satisfies both. The random phase wave form is transmitted using a Ritec RAM-10000 ultrasonic system, modified to accept arbitrary wave form excitation and perform automatic digital cross correlation on the measured response. A distinct advantage of the random phase signal over the chirp is that our signal transforms any system nonlinearity into time-domain noise that can be reduced by windowing. To obtain the impulse response of the ultrasonic system, the measured wave form from the detector is cross correlated with a stored replica of the transmitted excitation wave form. The correlated signal is equivalent to the response of the ultrasonic system to an elastic wave transient, and therefore can be treated like a conventional pulse wave form.

The measured time-domain wave forms $V(x,t)$ always contain interference signals not predicted by the above-given simplified analysis. At minimum, there are reflections and echos in the air between the transducers and the sample. In addition, our measurement system has a small, but detectable, leakage of the excitation signal into the detector circuit. Sound scattered from the source transducer can reflect from the measurement apparatus around the sample and appear at the detector. All of these interference signals are separated temporally from the desired plate mode wave forms. A key advantage of our time-domain measurement is our ability to eliminate interference by performing time-domain windowing.

The final step of our measurement procedure is to plot the two-dimensional spatial-temporal discrete Fourier transform of all of the correlated windowed time-domain wave forms. This step gives $V(k_x, \omega)$, our windowed measurement of the transmission coefficient. The magnitude of $V(k_x, \omega)$, plotted as a gray scale as a function of (k_x, ω) (or equivalently f and $k_x/2\pi$), is a spectrum of the transmission maxima of the medium. Because air is so tenuous, the transmission maxima essentially coincide with the Lamb modes of the medium, so the experimental result $V(k_x, \omega)$ is effectively a dispersion spectrum.

IV. RESULTS

We have reconstructed the dispersion relations of a wide variety of materials, but show only a few here for illustrative purposes. Figure 4 shows the dispersion relation of 6.68 mm 6061-T6 aluminum. The image is produced from a 300 mm scan in 2 mm steps in x with 3600 averages and the source and detector assemblies each rotated 2° to allow phase matching into as many modes as possible. Bright traces correspond to propagating Lamb modes. The lower frequency bound of the experiment is about 100 kHz and this can be seen in Fig. 4 as a sharp cutoff in the image background. The dashed curves in Fig. 4 are calculated from waveguide theory¹⁰ using nominal values for the elastic parameters of aluminum. Each curve corresponds to a different mode.

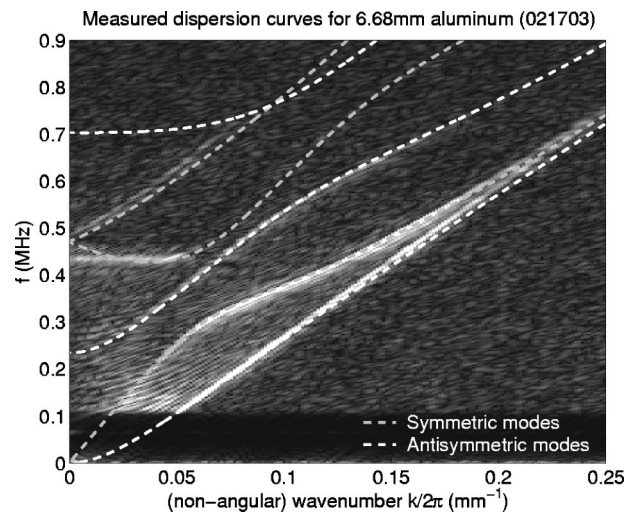


FIG. 4. Image of measured dispersion spectrum for aluminum, with superimposed dashed curves calculated from nominal elastic parameters. The horizontal axis, $k/2\pi$, is equivalent to $1/\lambda$.

Phase velocity of a mode at a particular frequency and wave number is ω/k or equivalently $f/(k/2\pi)$ and is determined by measuring the slope of the line from the origin to $(f, k/2\pi)$. Group velocity at a particular frequency and wave number is determined by measuring the slope of the dispersion curve $d\omega/dk$ [or equivalently $df/(dk/2\pi)$]. The dispersion curves shown in Fig. 4 correspond to, from bottom to top, the lowest order antisymmetric (A_0) and symmetric (S_0) modes, the first-order antisymmetric (A_1), first- and second-order symmetric (S_1 and S_2), and the second-order antisymmetric mode (A_2). Figure 4 shows the lowest order antisymmetric and symmetric modes very clearly. The first-order antisymmetric mode is clearly present, and the second-order symmetric mode is also clearly present in the measured data.

This scan was time consuming. Our equipment achieves a repetition rate of 15 Hz; this scan took approximately 10 h. Long scans and substantial averaging are required to achieve fine detail and optimum signal-to-noise ratio in the measured image. Nevertheless, even short scans with few averages can provide an adequate dispersion spectrum. We have achieved recognizable dispersion spectra in as little as 10 min.

Figure 5 shows the measured dispersion relation image for Lucite (poly methyl methacrylate), generated from a 160 mm scan in 2 mm steps with the transducers rotated to an angle of 7° with 4000 averages. Curves calculated from waveguide theory using nominal elastic parameters for Lucite¹³ are superimposed upon the curves shown in Fig. 5. These correspond to, from bottom to top, the A_0 , S_0 , A_1 , S_1 , S_2 , A_2 , S_3 , and A_3 modes. Every measured mode shows good alignment with the calculated curves. All of the modes except for the second-order antisymmetric and the third-order symmetric mode are visible in the measured dispersion relation image. Some portions of some modes appear brighter than others. Modes with large out-of-plane surface displacements will couple more efficiently to a pressure wave in the air. This fact explains why the upper portion of the S_0 mode beyond 0.07 mm^{-1} is so bright and almost disappears below 0.05 mm^{-1} . In addition, the transducer bandwidth and the spectral directivity of the rotated trans-

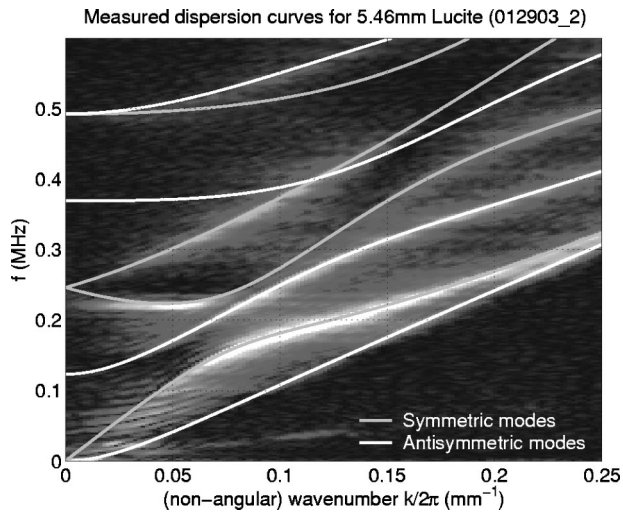


FIG. 5. Image of measured dispersion relation for Lucite, with superimposed curves calculated from nominal elastic parameters.

ducer limit the measurement region and thereby affect the intensities of the measured modes. Both Figs. 4 and 5 show the measured dispersion of the S_1 mode below 0.05 mm^{-1} to be nearly horizontal, whereas the theoretical curve increases toward the axis. This phenomenon is the well-known negative group velocity mode. In fact, a full three-dimensional reconstruction of the dispersion spectrum, utilizing spatial scanning in both x and y , yields curves which follow precisely the calculation. The horizontal segment that appears in Figs. 4 and 5 is therefore an artifact caused by the finite extent in y of the line source. This interesting effect has significant implications for scanned imaging, and we have taken this up in another publication.¹⁴

Figure 6 shows a synthetic dispersion spectrum analogous to the 5.46 mm Lucite of Fig. 5 calculated using Eq. (11). It is the transmission coefficient, calculated using well-known theory,¹⁰ and multiplied by the transducer response, similar to Fig. 3, but measured with a transducer rotation angle of 6° . The calculation was done based on the same elastic parameters used to calculate the dispersion curves of

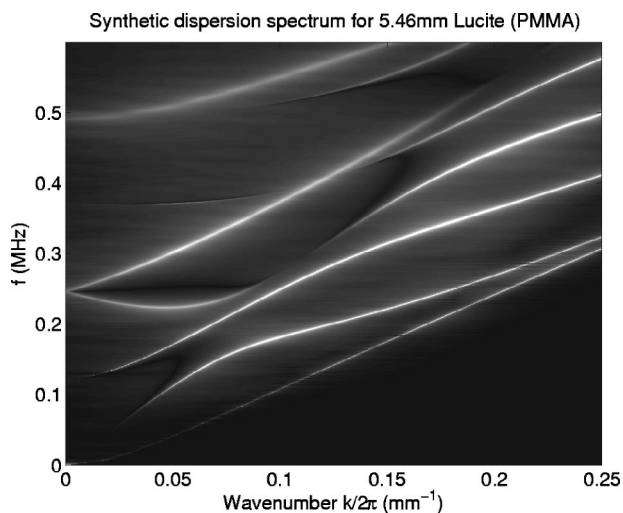


FIG. 6. Synthetic dispersion spectrum for Lucite, calculated according to Eq. (11).

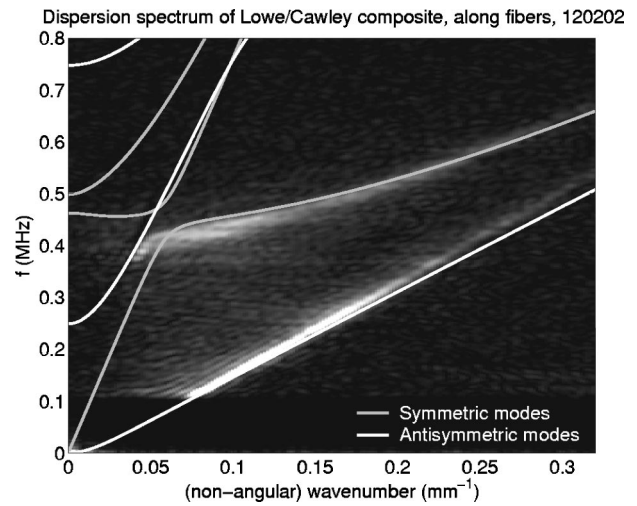


FIG. 7. Measured dispersion spectrum of uniaxial carbon fiber, parallel to fiber direction.

Fig. 3, and with published viscoelastic attenuation values.³ More modes are visible here than in Fig. 3 because of the perfect signal-to-noise ratio, but they appear in the same places and many have similar intensity ratios. We note that the flat spot in the S_1 mode discussed earlier does not appear. That is because this calculation is based on a two-dimensional model that assumes the transducer to be infinite in y . The flat spot was caused by using a three-dimensional transducer in a two-dimensional model.

We can measure dispersion spectra of anisotropic materials as well. In this case, the measured spectra will depend on the selected direction of propagation. Figure 7 shows a measured dispersion spectrum (1500 averages) for propagation along the fibers of a sample of 3.3-mm-thick uniaxial carbon fiber epoxy laminate. For this measurement the transducer assemblies have been rotated to 6° . Superimposed on the data are dispersion curves calculated from independently measured elastic constants. The A_0 and S_0 modes are clearly visible, although the lower frequencies and initial slope of the S_0 are not, for reasons pointed out earlier. The sharp knee in the S_0 at around 0.06 mm^{-1} and 0.4 MHz is a consequence of the high elastic anisotropy typical of these materials. Figure 8 shows the measured spectrum for propagation normal to the fiber direction of the same sample, this time with the transducer assemblies again rotated to 6° , and again with 1500 averages. Here, A_0 , S_0 , A_1 , and S_2 modes are all clearly visible in the locations predicted by the theoretical calculations. The modal structure in this case is indicative of an isotropic sample, because we are measuring in the composite's plane of isotropy.

Figure 9 shows a dispersion spectrum for a 9.53-mm-thick balsa wood plate, measured with 2400 averages. In this case we have been able to image both the zeroth-order and many higher order modes. The effect of anisotropy of the wood is also clearly visible in these curves, as it was in the case of the composite. Because wood is a natural fiber, elastic property variations can occur from point to point. Therefore, the data in Fig. 9 are less well defined than for the engineering materials presented earlier. Nonetheless, the structure of the higher order modes is clear and both the

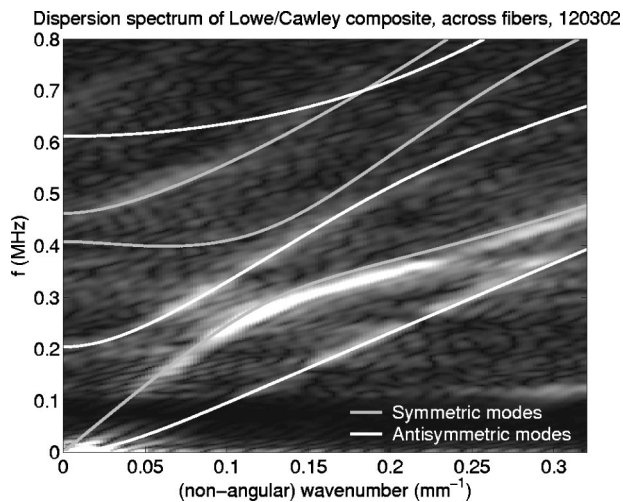


FIG. 8. Measured dispersion spectrum of uniaxial carbon fiber, perpendicular to fiber direction.

longitudinal wave speed and Rayleigh wave asymptote are clearly visible in the data of Fig. 9

V. CONCLUSIONS

We have demonstrated in this paper a noncontact method using air-coupled focused ultrasound to deduce the dispersion characteristics of isotropic and anisotropic plates. By combining random phase excitation and correlation with synthetic aperture scanning we can reconstruct entire portions of a dispersion spectrum in a single scan. The large number of inflection points in the dispersion curves visible in the images shown in Sec. IV allow a robust and reliable

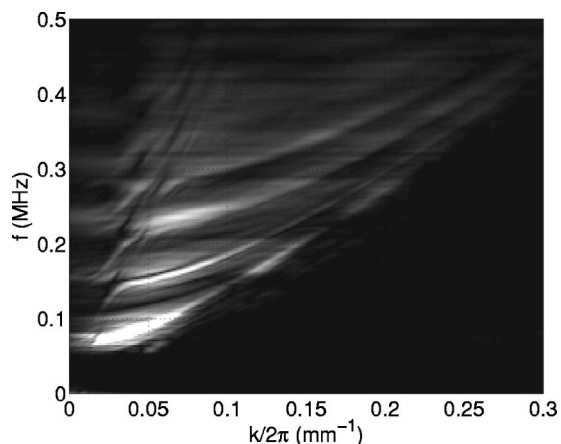


FIG. 9. Experimental dispersion spectrum of 9.53 mm balsa wood, measured along the grain.

fitting procedure. The high sensitivity of certain dispersion curve segments to particular elastic constants is well established.^{8,15} Unlike many previous methods, our results can be compared directly with calculations from waveguide theory. Assumptions (except for line-focus) about the acoustic beam function of the transducers are not required.

The several examples shown here serve to illustrate the capability of this technique. We have reconstructed the dispersion relations of a wide variety of materials, including anisotropic composites and even wood. There is nothing in principle that limits applicability of this method to measuring guided Lamb waves in plates; the dispersion characteristic of any leaky ultrasonic guided mode can be measured in this way. The noncontact nature of the procedure presented here opens possibilities for examining materials which cannot be immersed in coupling liquids.

- ¹W. Khul, G. R. Schodder, and F. K. Schröder, "Condenser transmitters and microphones with solid dielectric for airborne ultrasonics," *Acustica* **4**, 519–532 (1954).
- ²M. Luukkala, P. Heikkilä, and J. Surakka, "Plate wave resonance—A contactless test method," *Ultrasonics* **9**, 201–208 (1971).
- ³A. Safaeinili, O. I. Lobkis, and D. E. Chimenti, "Air-coupled ultrasonic estimation of viscoelastic stiffness in plates," *IEEE Trans. Ultrason. Ferroelectr. Freq. Control* **43**, 1171–1180 (1996).
- ⁴W. A. Grandia and C. M. Fortunko, "NDE applications of air-coupled ultrasonic transducers," *Proceedings of the 1995 IEEE Ultrasonics Symposium*, pp. 697–709.
- ⁵D. W. Schindel, D. A. Hutchins, L. Zou, and M. Sayer, "The design and characterization of micromachined air-coupled capacitance transducers," *IEEE Trans. Ultrason. Ferroelectr. Freq. Control* **42**, 42–50 (1995).
- ⁶I. Ladabaum and B. T. Khuri-Yakub, "Micromachined ultrasonic transducers: 11.4 MHz transmission in air and more," *Appl. Phys. Lett.* **68**, 7–9 (1996).
- ⁷B. Hosten and M. Castaings, "Parabolic mirror and air-coupled transducer for multimodal plate wave detection," in *Review of Progress in Quantitative Nondestructive Evaluation*, edited by D. O. Thompson and D. E. Chimenti (AIP Press, New York, 2002), Vol. 22, pp. 1243–1250.
- ⁸D. Fei and D. E. Chimenti, "Single-scan elastic property estimation in plates," *Acoustics Res. Lett. Online* **2**, 49–54 (2001).
- ⁹G. A. Deschamps, "Gaussian beam as a bundle of complex rays," *Electron. Lett.* **7**, 684–685 (1971).
- ¹⁰A. N. Nayfeh, *Wave Propagation in Layered Anisotropic Media* (Elsevier, Amsterdam, 1995).
- ¹¹B. A. Auld, *Acoustic Fields and Waves in Solids*, 2nd ed. (Krieger, Malabar, FL, 1990), Vol. II.
- ¹²T. H. Gan, D. A. Hutchins, D. R. Billson, and D. W. Schindel, "The use of broadband acoustic transducers and pulse-compression techniques for air-coupled ultrasonic imaging," *Ultrasonics* **39**, 181–194 (2001).
- ¹³B. Hartmann and J. Jarzynski, "Immersion apparatus for ultrasonic measurements in polymers," *J. Acoust. Soc. Am.* **56**, 1469–1477 (1974).
- ¹⁴S. D. Holland and D. E. Chimenti, "Air-coupled acoustic imaging with zero-group-velocity Lamb modes," *Appl. Phys. Lett.* **83**, 2704–2706 (2003).
- ¹⁵D. E. Chimenti and D. Fei, "Scattering coefficient reconstruction in plates using focused acoustic beams," *Int. J. Solids Struct.* **39**, 5495–5513 (2002).